



Contents

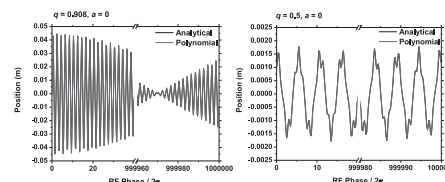
Regular articles

73–80

Minimized computational time method for the dynamics of ions trapped in an ideal quadrupole ion trap

Mustapha Said Herbane

- Power series solution of the Mathieu equation. ► Minimization of the computational time.
- Numerical solution for the excited ions and buffer gas cooling.

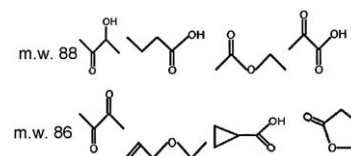


81–89

Selected ion flow tube, SIFT, studies of the reactions of H_3O^+ , NO^+ and O_2^+ with some biologically active isobaric compounds in preparation for SIFT-MS analyses

David Smith, Thomas W.E. Chippendale, Patrik Španěl

- Data are reported for SIFT-MS quantification of eight biologically active compounds. ► Isobaric compounds can be distinguished by hydration of characteristic product ions. ► Pyruvic acid can be analysed in the headspace of its aqueous solution using SIFT-MS. ► Acetoin and diacetyl are quantified in the headspace above incubated yoghurt.

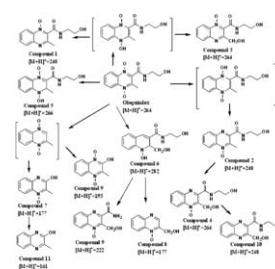


90–96

Structural elucidation of degradation products of olaquinox under stressed conditions by accurate mass measurements using electrospray ionization hybrid ion trap/time-of-flight mass spectrometry

Zhao-Ying Liu, Hua-Hai Zhang, Xiao-Jun Chen, Xiao-Ni Zhou, Leren Wan, Zhi-Liang Sun

- The stress degradation of olaquinox is investigated by LC/MS-IT-TOF. ► A total of 12 degradation products are characterized. ► A comprehensive degradation pathway of olaquinox is tentatively outlined. ► The use of LC/MS-IT-TOF approach appears to be rapid and efficient in structural identification.

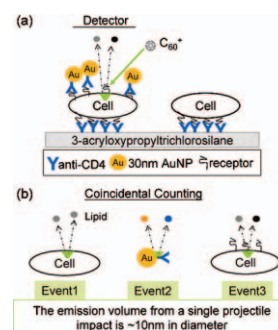


97–102

Characterization and quantification of nanoparticle–antibody conjugates on cells using C_{60} ToF SIMS in the event-by-event bombardment/detection mode

Li-Jung Chen, Sunny S. Shah, Jaime Silangcruz, Michael J. Eller, Stanislav V. Verkhoturov, Alexander Revzin, Emile A. Schweikert

► Illustrate the ability of Cluster C_{60} ToF-SIMS in the individual impact mode. ► Validate the immobilization of AuNP labeled antiCD4 on cell surfaces. ► Quantify the coverage/density of molecules/nanoprobe immobilized on cell surfaces.

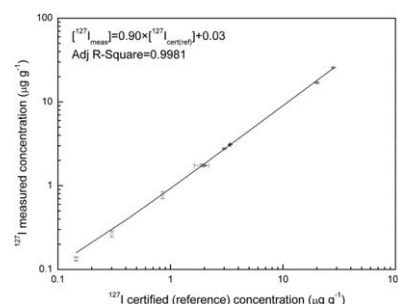


103–108

Microwave-based digestion method for extraction of ^{127}I and ^{129}I from solid material for measurements by AMS and ICP-MS

J.M. Gómez-Guzmán, S.M. Enamorado-Báez, A.R. Pinto-Gómez, J.M. Abril-Hernández

► A microwave digestion to extract iodine from environmental matrices was developed. ► Samples were digested using HNO_3 looking for shorter preparation times. ► The method was tested measuring ^{127}I by ICP-MS in standard reference materials. ► The chemical recovery was found to be about 90%. ► Validation was made measuring by AMS three CRM's with known concentrations of ^{129}I .

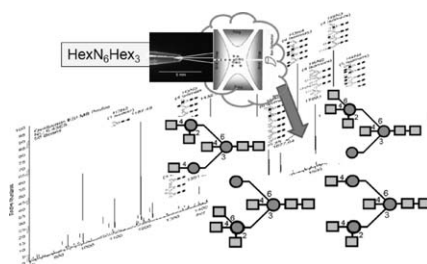


109–117

High performance IT-MSⁿ sequencing of glycans. Spatial resolution of ovalbumin isomers

Jenny Jiao, Hailong Zhang, Vernon N. Reinhold

► Non-chromatographic, high performance spatial approach to resolve the N-glycans of ovalbumin. ► IT-MSⁿ disassembly with fragment ion library confirmation. ► Sequencing technology patterned to be comprehensive, and stay within the bounds of a plausible high throughput strategy consistent with automation. ► Considerations may offer some reprieve from this two-century-old problem of carbohydrate sequencing.

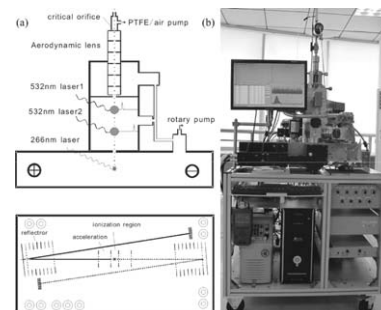


118–124

Real time bipolar time-of-flight mass spectrometer for analyzing single aerosol particles

Lei Li, Zhengxu Huang, Junguo Dong, Mei Li, Wei Gao, Huiqing Nian, Zhong Fu, Guohua Zhang, Xinhui Bi, Ping Cheng, Zhen Zhou

► A new built aerosol mass spectrometer capable of determining the size and chemical compositions of individual particles ranging from 250 nm to 2000 nm in real-time and achieving a total hit rate above 30%. ► The mechanical structure of the instrument is compact and the vacuum system is simplified. ► Bipolar grid reflectron mass analyzers with ion focus technology increase the mass resolution and ion transmission efficiency. ► The preliminary ambient aerosol detection shows that it has great potential applications in environmental aerosol measurements and laboratory aerosol mechanics researches in China.

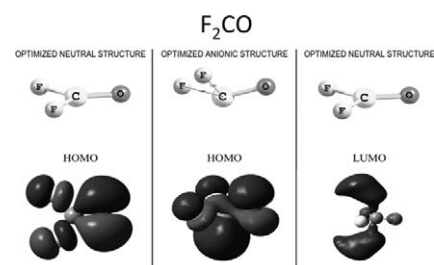


125–128

Dissociative electron attachment to carbonyl fluoride, F_2CO

M. Hoshino, P. Limão-Vieira, M. Probst, Y. Nunes, H. Tanaka

► Dissociative electron attachment to F_2CO . ► Formation of fragments with the most dominant DEA reaction leading to F^- . ► Plasma processing molecule replacement. ► Quantum chemical calculations on the electronic properties of F_2CO .

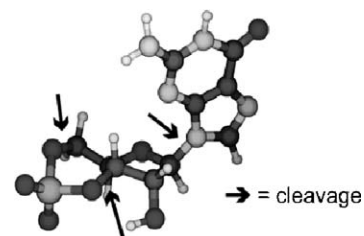


129–136

UV-photodissociation of non-cyclic and cyclic mononucleotides

Jesse C. Marcum, Sydney H. Kaufman, J. Mathias Weber

► Photodissociation of cyclic mononucleotides after UV excitation occurs predominantly by loss of anionic base. ► Decay of RNA and DNA mononucleotides is dominated by loss of neutral base and loss of phosphate-based anions. ► Differences between cyclic and non-cyclic fragmentation pathways can be attributed to different tethering of the phosphate group. ► The presence of different functional groups on the phosphate-sugar “backbone” of cyclic and non-cyclic nucleotides does not affect the envelope of the electronic spectra of adenosine and guanosine-based nucleotides.

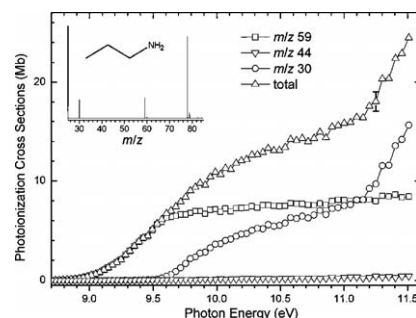


137–146

Determination of absolute photoionization cross-sections of nitrogenous compounds

Mingfeng Xie, Zhongyue Zhou, Zhandong Wang, Dongna Chen, Fei Qi

► Nitrogenous compounds can be found in coal, heavy oils and solid fuels from biomass to waste. ► Quantification of combustion species of these compounds is of great importance. ► We determined absolute photoionization cross-sections of 24 nitrogenous compounds. ► The data are important for quantification analysis of combustion intermediates.

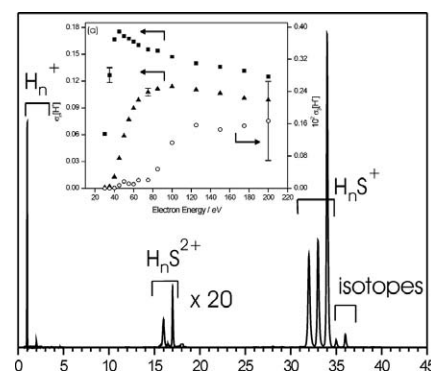


147–153

Electron ionization of hydrogen sulfide

Kevin M. Douglas, Stephen D. Price

► The various fragment ions formed by electron ionization of H_2S have been quantified. ► The contribution of multiple ionization to the fragment ion yield is measured. ► Energetics and fate of the excited electronic states of H_2S^{2+} are revealed. ► Above 50 eV, most H_2S^{2+} fragmentations involve excited dicationic states.

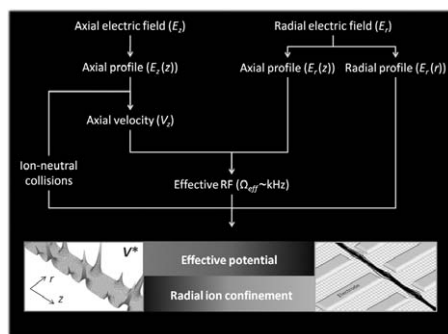


154–163

Gas-phase ion dynamics in a periodic-focusing DC ion guide (Part II): Discrete transport modes

Chaminda M. Gamage, Joshua A. Silveira, Ryan C. Blase, David H. Russell

► Discrete ion transport modes in a PDC IG(axial drift, radial ripple, and central drift motion) are deconvoluted and discussed. ► Equations of motion are derived to mathematically explain ion motion in the axial and radial directions. ► The results support the radial focusing model based on a collisionally dampened effective potential. ► Derivation of ion-neutral collision cross sections using first-order IMS principles is discussed.

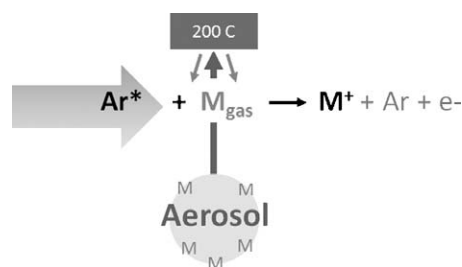


164–172

Thermal desorption metastable atom bombardment ionization aerosol mass spectrometer

Carly B. Robinson, Joel R. Kimmel, Donald E. David, John T. Jayne, Achim Trimborn, Douglas R. Worsnop, Jose L. Jimenez

► Metastable atom beam source coupled to a field deployable TOFMS. ► Penning ionization of thermally desorbed aerosols. ► Laboratory and field characterization of performance.

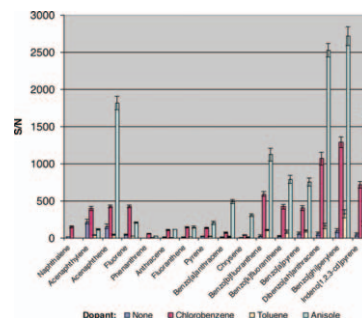


173–180

Liquid chromatography/dopant-assisted atmospheric pressure chemical ionization mass spectrometry for the analysis of non-polar compounds

Liguo Song, David S. Cho, Deepak Bhandari, Stephen C. Gibson, Mary Ellen McNally, Ron M. Hoffman, Kelsey D. Cook

► LC/DA-APCI-MS was introduced for the analysis of non-polar compounds, i.e., PAHs. ► Chlorobenzene, toluene, anisole were explored as dopants. ► Predominant M^{++} ions were observed for fourteen of the sixteen U.S.EPA priority PAHs. ► Predominant $[M-H]^{++}$ ions were observed for acenaphthene and fluorene. ► Anisole was the best dopant with improved S/N up to two orders of magnitude.

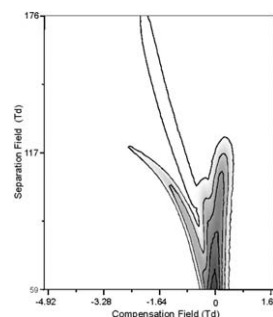


181–190

Gas phase fragmentation of protonated esters in air at ambient pressure through ion heating by electric field in differential mobility spectrometry

X. An, G.A. Eiceman, J.E. Rodriguez, J.A. Stone

► Ions were fragmented in a differential mobility spectrometry at ambient pressure. ► Decomposition was effected by temperature plus applied electric field. ► Electric field equivalence was 1.5°C per Townsend. ► Electric field threshold for decomposition is mass dependence.

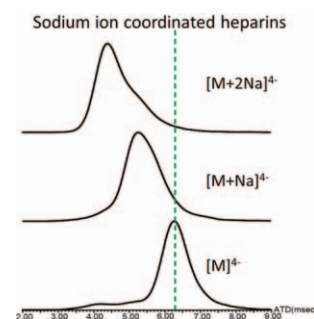


191–198

Biologically relevant metal-cation binding induces conformational changes in heparin oligosaccharides as measured by ion mobility mass spectrometry

Youjin Seo, Matthew R. Schenauer, Julie A. Leary

► Collision cross sections of heparin octasaccharides coordinated with and without metal ions were determined using ion mobility mass spectrometry. ► Metal ions induce a conformational change of heparin octasaccharide structure. ► Conformational changes observed in the gas phase with calcium ion coordinated heparin octasaccharide were consistent with that in solution.

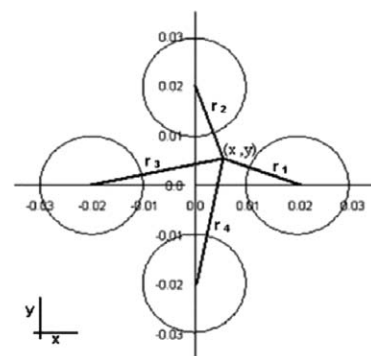


199–205

Distribution into the quadrupole mass filter with round rods

F. Kashanian, S. Nouri, S. Seddighi Chaharborj, A.B. Mohd Rizam

► Potential field distribution of a quadrupole mass filter with circular cross-section electrodes is described. ► Using superposition principle, we calculate potential around a round rod which is subjected to a given potential. ► By standard separation method, we obtain the potential distribution into the quadrupole mass filter with circular rods. ► Same equivalent operating point in two stability diagrams (having the same β_y) the associated modulated secular ion frequencies behavior are the same.

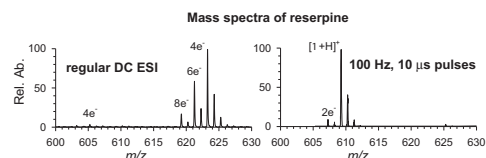


206–211

Control of analyte electrolysis in electrospray ionization mass spectrometry using repetitively pulsed high voltage

Vilmos Kertesz, Gary J. Van Berkel

► Pulse parameters in ESI-MS using pulsed high voltage affect analyte electrolysis. ► Exclusive electrolysis of the solvent proximal to the electrode is possible. ► Novel simple electronic means to control analyte electrolysis in ESI-MS.

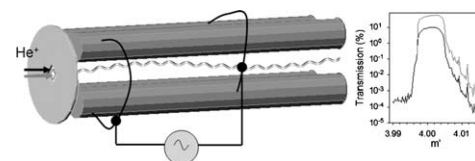


212–219

Comparison of quadrupole mass filters with hyperbolic and cylindrical rods working in the third stability zone

Gianangelo Bracco

► Quadrupole mass filters with cylindrical and hyperbolic rods. ► Comparison of transmission and mass resolution in the third stability zone. ► Reduced injection region increases transmission and avoid low mass tail. ► High mass tails reduced by a frequency increase. ► Same baseline resolution and transmission for cylindrical and hyperbolic rods.

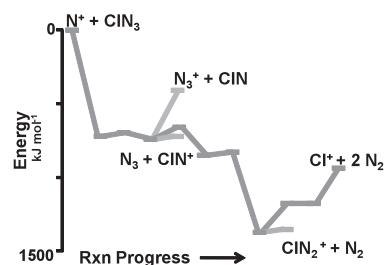


220–224

Reactions of positive ions with ClN_3 at 300 K

Nicole Eyet, Keith Freel, Michael C. Heaven, A.A. Viggiano

- The kinetics of eighteen positive ions with chlorine azide(ClN_3) have been studied.
- The ionization energy of ClN_3 $> 930 \text{ kJ mol}^{-1}$ ($> 9.6 \text{ eV}$). ► The proton affinity of ClN_3 is $713 \pm 41 \text{ kJ mol}^{-1}$.
- A reaction coordinate diagram for the novel reaction of N^+ with ClN_3 is discussed.



225–228

Fast identification of phthalic acid esters in poly(vinyl chloride) samples by Direct Analysis In Real Time (DART) tandem mass spectrometry

Ákos Kuki, Lajos Nagy, Miklós Zsuga, Sándor Kéki

- Mass-dependent tuning of the collision energy/voltage in DART-MS/MS was achieved. ► We report a highly automated data acquisition method for DART-MS/MS. ► A fast screening technique for the detection of plasticizers in PVC was developed.

